ELSEVIER

Journal of Physics and Chemistry of Solids 64 (2003) 1453–1459

JOURNAL OF PHYSICS AND CHEMISTRY OF SOLIDS

www.elsevier.com/locate/jpcs

Advanced tetrahedrally-bonded magnetic semiconductors for spintronic applications

A.J. Freeman*, Yu-Jun Zhao

Department of Physics and Astronomy, Northwestern University, Evanston, IL 60208, USA

Abstract

Recent developments of magnetic semiconductors suggest the possibility of harnessing the spin of the electron —in addition to its charge—for future devices and some examples are given here. Highly precise FLAPW calculations demonstrate that: (i) $Cd_{1-x}Mn_xGeP_2$ chalcopyrites are antiferromagnetically (AFM) favored but will undergo a phase transition to the FM state with n-type S doping. Hence, the magnetic moments (mm) may be tuned with impurities, and a great boon for technological applications; (ii) a new class of half-metallic ferromagnetic semiconductors in Mn doped I–III–VI_2 chalcopyrites is predicted with the Curie temperature T_C proportional to the hole concentration. Moreover, we investigated the electronic and magnetic properties of Mn_xGe_{1-x} as a function of Mn positions in a 64 atom supercell. The FM aligned Mn at a distance of $a\sqrt{2}$ has the lowest energy, followed by several energetically competitive FM and AFM configurations, explaining the observation of 'inactive' Mn mm, and the theoretical mm of 3.0 μ_B per Mn for the FM states. Surprisingly, the exchange interaction between a Mn pair is found to oscillate with the distance between them, and to obey the RKKY analytic formula. In addition, the estimated T_C, around 134–400 K, is in good agreement with experiment.

Keywords: A Semiconductors

1. Introduction

Spintronics is spin based electronics, where it is not only the electron charge but the electron spin that carries information, and this offers opportunities for a new generation of devices [1]. In comparison with conventional semiconductor devices, spintronic devices are promising in improving data processing speed, reducing electric power consumption and increasing integration densities [1]. Due to the great advantages in possible electronic devices, intensive attention has been paid to semiconductor based ferromagnetic (FM) materials, including Mn doped III–V [2,3], group IV [4], and chalcopyrite [5,6] semiconductors. Although room-temperature ferromagnetism was observed in several Mn doped semiconductors [5,7,8], there is still lacking ideal spintronic materials with not only room temperature ferromagnetism, but also efficient spin injection, easy control of transport, etc. On the other hand, the origin of the ferromagnetism in magnetic semiconductors is under intense discussion [9], with many mechanisms proposed, including Ruderman–Kittel–Kasuya–Yosida (RKKY) [10], and double resonance mechanisms [11].

Here, we review our recent high precisely first-principles calculations on: (i) possible impurity induced ferromagnetism in Mn doped II-Ge–V_2 chalcopyrite; (ii) prediction of a new class of FM semiconductor based on I–III–VI_2 chalcopyrite; and (iii) the nature and origin of ferromagnetism in a very recent discovered magnetic semiconductor-homonuclear Ge doped with Mn.

2. Impurity induced FM in Mn doped II–VI–V_2

While the observed ferromagnetism and the attractive injection phenomena are essentially limited to low temperatures in Mn doped GaAs and InAs semiconductors, II-Ge–V_2 chalcopyrites have drawn considerable attention due to their chemical similarity to the III–V semiconductors. In II-Ge–V_2 chalcopyrites, the II–IV combination plays the role of two group-III atoms, and jointly supply three valence electrons per atom, to combine with the five electrons

* Corresponding author. Fax: +1-847-4915082.
E-mail address: art@freeman.phys.nwu.edu (A.J. Freeman).

0022-3697/03/$ - see front matter © 2003 Elsevier Ltd. All rights reserved.
doi:10.1016/S0022-3697(03)00120-3

provided by each group-V ion. The expected special advantage of these systems is that Mn can be substituted readily for II cations, as demonstrated [12] for $II_{1-x}Mn_xIV$ alloys with x up to 1.0 without the formation of structural defects, owing to the natural tendency of Mn to adopt a +2 state.

The first FM semiconductor based on II-Ge–v_2 was reported by Medvedkin et al. [5]; they obtained room temperature ferromagnetism in highly doped $Cd_{1-x}Mn_xGeP_2$—which constitutes a tremendous improvement from the T_C of 110 K found in $Ga_{1-x}Mn_xAs$ for $x = 0.053$. Very recently, Cho, et al. [7] found another room temperature FM semiconductor in II-Ge–V_2 chalcopyrite $Zn_{1-x}Mn_xGeP_2$ with $T_C = 312$ K.

However, our first-principles theoretical calculations [6,13] on Mn doped ordered $CdGeP_2$, $ZnGeP_2$, $CdGeAs_2$, and $ZnGeAs_2$ systems showed that the total energy of the AFM state is lower than the corresponding FM state for all these systems. More recently, Mahadevan and Zunger [14] gave a possible explanation for the ferromagnetism in Mn doped $CdGeP_2$. They found that low energy intrinsic defects may provide holes and stabilize the FM coupling between Mn ions. There are still unexplained phenomena in these Mn doped II-Ge–V_2; for example, the energy gap was enlarged and no carriers were observed [5] due to Mn doping in experiment, which the theoretical calculations did not support [13,14]. Thus, careful characterizations on Mn doped II-Ge–V_2 are still called for.

In order to control the magnetism and carriers independently, other possible ways to stabilize the FM coupling between Mn ions in Mn isovalently doped semiconductors were investigated [15]. We investigated the possible AFM–FM transition induced by impurities in $II_{1-x}Mn_xGeV_2$ systems with the full-potential linearized augmented plane wave (FLAPW) [16] method within the generalized gradient approximation (GGA) [17], exemplified by $Cd_{1-x}Mn_xGeP_2$. (The geometry structure optimization and formation energy calculations were done by the $DMol^3$ method [18] in order to save computational efforts). To begin with, Si and S are easily seen to be good choices for impurity induced carriers, since they are the same row neighbors of P in the periodic table. First, we calculated the formation energy for Si or S substituting P or Ge sites with a $Cd_3MnGe_4P_8$ unit cell, i.e. $x = 0.25$. The formation energy H_f of a defect α is generally a function of Fermi energy E_F atomic chemical potentials μ_i, and charge state q [19,20]

$$H_f(\alpha, q) = \Delta E(\alpha) - E(0) + \sum_i n_i \mu_i + qE_F, \quad (1)$$

where $E(\alpha)$ and $E(0)$ are the total energies of the supercell with and without defect α and n_i is the number of each defect atom related to the chemical reaction formation of defect α. Here we only consider neutral defects of S or Si substituting P or Ge sites and all the chemical potentials are from their elemental crystals [6]. The calculated formation energies for the possible substitutions are listed in Table 1.

Table 1
The calculated formation energy, H_f (eV), for Si and S substituting the P or Ge sites in $Cd_{1-x}Mn_xGeP_2$ at $x = 0.25$. P1 represents the P sites close to Mn, and P2 represents other P sites. In the calculations, the internal structures are fully optimized, while the lattice volume is assumed to be the same as that without S or Si impurities

Impurity	P1	P2	Ge
Si	1.37	1.47	−0.52
S	0.14	0.16	1.80

We found that while Si goes easily into the Ge site rather than the P site because their valences match, this will not be helpful in producing carriers. On the other hand, S prefers P sites rather than Ge sites with H_f around 0.14 eV. We assume that S could be doped into $Cd_{1-x}Mn_xGeP_2$ at certain concentrations, and study the effect of its doping on the magnetic properties of $Cd_{1-x}Mn_xGeP_2$.

With 12.5% P substituted by S, the internal structures of FM and AFM $Cd_{1-x}Mn_xGeP_2$ are optimized with the AFM configurations set in the same 'spin superlattice' as before. The FLAPW total energy difference between FM and AFM states for $x = 0.25$, 0.5 and 1.0 are shown in Fig. 1. For $x = 1.0$, $Cd_{1-x}Mn_xGeP_2$ still keeps AFM as its stable phase, but the energy difference from the FM phase is reduced by ~72 meV/Mn when S is introduced. For $x = 0.25$ and 0.50, the total energy of the FM state becomes lower than that of the AFM state, i.e. an AFM to FM phase transition is found due to S doping.

To examine the effect of S doping on the electronic structures, the total DOS and projected Mn 3d DOS for $x = 0.50$ are shown in Fig. 2. Obviously, the Fermi level is

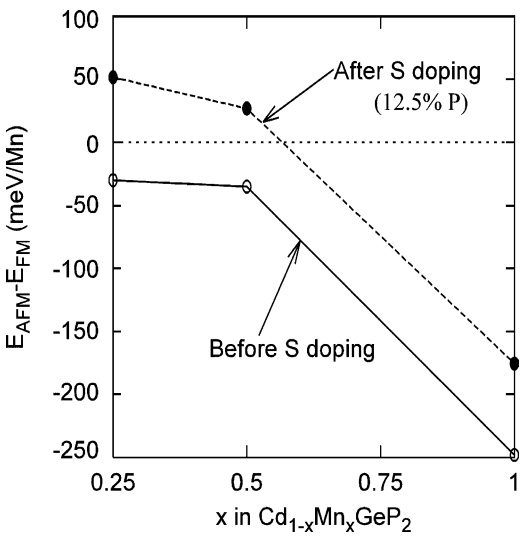

Fig. 1. The total energy difference between AFM state and FM state for $CdMn_{0.5}Ge_{0.5}P_2$ before (solid line) and after (dashed line) substituting 12.5% P by S.

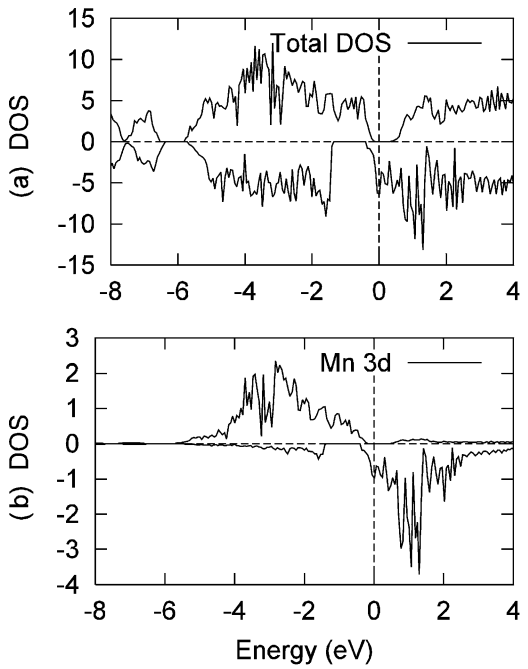

Fig. 2. (a) The total density of states (DOS) and (b) projected Mn 3d DOS for $CdMn_{0.5}Ge_{0.5}P_2$ with 12.5% P substituted by S.

shifted to higher energy due to the additional electron introduced by S substituting P. The total DOS indicates that the additional electron fills in the spin down bands, and makes the system half-metallic. Therefore, each doped S will reduce the magnetic moment of the system by one μ_B: the calculated total magnetic moments come out to be 4.5 μ_B per Mn for $x = 0.50$ and 4.0 μ_B per Mn for $x = 0.25$, respectively, due to the corresponding Mn/S ratio (2:1 for $x = 0.50$ and 1:1 for $x = 0.25$). That is the total magnetic moment obeys the following equation

$$M = (5 - N_S/N_{Mn})\mu_B/\text{Mn}. \quad (2)$$

In order to see the effect of S concentration, we also studied $Cd_{1-x}Mn_xGeP_2$ for $x = 0.25$ with P substituted by 6.25% S. The calculated energy difference between FM and AFM is 40.0 meV/Mn, i.e. very close to that of the 12.5% S case. This confirms that the AFM to FM phase transition will also occur at lower S concentration. The total magnetic moment for $Cd_{0.75}Mn_{0.25}GeP_{1.875}S_{0.125}$ is 4.5 μ_B/Mn, in excellent agreement with Eq. (2).

As a result, the total magnetic moments may be tuned easily by the impurity concentrations, which may be a great boon for technological applications. The projected DOS shows that the Mn 3d spin up bands are fully occupied and the spin down bands are partially filled due to the shift of E_F; the S 3p bands are also strongly spin-split due to hybridization with the Mn 3d bands. The fact of an induced magnetic transition once again shows the important role of carriers in FM semiconductors. Moreover, the n-type FM induced by S is also interesting for spintronic applications since n-type devices have longer lifetimes than do p-type devices.

3. Prediction of ferromagnetism in I–III–VI_2 chalcopyrites

In the search for new FM semiconductors, we turned to a new class of I–III–VI_2 chalcopyrite semiconductors, such as Mn doped $CuGaSe_2$, $CuGaS_2$, and $CuAlS_2$ [21,22]. Our first-principles calculations, performed with both the FLAPW [16] and $DMol^3$ methods [18] within GGA [17] to density functional theory, predicted them to be a new class of FM semiconductors with Curie temperatures of 80–180 K. While T_C may be lower for smaller x and still too low for applications, this finding opens the possibility of discovering other I–III–VI_2 materials with higher Curie temperatures.

The reason we chose the I–III–VI_2 chalcopyrite as a host semiconductor is based on the contrast between $Ga_{1-x}Mn_xAs$ and $Cd_{1-x}Mn_xGeP_2$. It is well known that carriers are necessary to make the Mn atoms couple ferromagnetically in semiconductors. Clearly, Mn in $Ga_{1-x}Mn_xAs$, which goes in at the +3 cation site, forms defect bands and provides holes to make the nonmagnetic semiconductor FM [23]. In the case of $Cd_{1-x}Mn_xGeP_2$, the valence of the Mn ion matches that of the host, and results in AFM coupling. In the cases of $CuGaSe_2$, $CuGaS_2$, and $CuAlS_2$, we expected that Mn would substitute on the Ga site and so provide holes and make the host semiconductor FM—as in GaAs.

This conjecture was tested using first-principles total energy calculations of the formation energy, H_f, with the $DMol^3$ method in a 16-atom unit cell. Then the formation energy is calculated according to Eq. (1) for the neutral charged defects of Mn substituting a single cation (namely Cu, Ga, or Al) in the pure chalcopyrites and the chemical potentials of the atoms are calculated from their elemental crystals [21]. From Table 2, we know that the calculated H_f of Mn substituting for Ga is lower than that for Cu in $CuGaSe_2$ and $CuGaS_2$. This indicates that Mn substitutes into the Ga site rather than the Cu site in $CuGaSe_2$ and $CuGaS_2$. For $CuAlS_2$, Mn is easier to substitute for Cu than for Al, which may be attributed to the size mismatch of Mn at Al site. The calculated energy of formation for Mn

Table 2
The calculated formation energy (eV/Mn)

Mn →	Cu	Ga	Al
$CuGaSe_2$	0.73	0.48	
$CuGaS_2$	0.80	0.43	
$CuAlS_2$	0.96		1.45

Table 3
DMol^3 calculated total energy difference between the AFM state and corresponding FM state, ΔE_{ex} as a function of the Mn concentration x for different ordering direction **G** and period p of spin superlattices

σ	p	**G**	ΔE_{ex}	
			$CuGaSe_2$	$CuGaS_2$
$x = 0.5$(I)	1	[001]	96.4	89.4
$x = 0.5$(II)	2	[100]	93.4	87.0
$x = 0.25$	1	[100]	80.5	84.8
$x = 0.125$	1	[100]	63.6	76.8

substituting Ga is its upper limit. If the system is Ga-poor, the energy of formation may be lower. (For comparison, we also calculated E_F for Mn substituting Ga in the (Ga, Mn)As system under similar conditions. The DMol^3 calculated E_F in $Ga_{1-x}Mn_xAs$ for $x = 12.5\%$ is 0.52 eV/Mn, which is higher than that in $CuGa_{1-x}Mn_xSe2$ and $CuGa_{1-x}Mn_xS_2$, indicating that similar or higher Mn solubility may be achieved in comparison with $Ga_{1-x}Mn_xAs$, for which x limited to 7.1%).

To determine the favored magnetic ordering and Curie temperature, one has to calculate the exchange interaction energy between nth nearest-neighbors, $J_n(x)$. The values of $J_n(x)$ were calculated from these total energy differences along with an empirical power law dependence of $J_n(x)$. on distance suggested by Twardowski et al. [24]. For each concentration x, we performed total energy calculations by DMol^3 (later checked [21,22] by the FLAPW method) for one or two AFM configurations, and the FM configuration, yielding the exchange interaction energies for Mn doped $CuGaSe_2$ and $CuGaS_2$ listed in Table 3. Clearly, the total energy calculations shows that FM states are preferred for both systems at different Mn concentrations, i.e. a new class of FM semiconductors are predicted on Mn doped I–III–VI_2 chalcopyrites.

Now, the optimum way to estimate the Curie temperature is still an open question even if the exchange constants $J_n(x)$ are obtained. One way to estimate the order–disorder transition temperature T_C from the calculated $J_1(x)$. is to make use of the Monte Carlo simulation for the nearest-neighbor classic Heisenberg Hamiltonian. Here, we employ the Monte Carlo simulation results for $Cd_{1-x}Mn_xTe$, which has the zinc-blende structure [25], namely, $T_C = 0.447|J_1|$. With the $J_1(x)$ obtained from Table 3, the estimated T_C's for Mn doped $CuGaSe_2$ and $CuGaS_2$ as a function of Mn concentration are shown in Fig. 3 with T_C ranging from 80 to 180 K. Obviously, the systems with greater Mn concentration has a higher T_C, and Mn doped $CuGaS_2$ has a higher T_C than that of $CuGaSe_2$ for the same Mn concentration. These results are in good agreement with the suggestions [10] by Deitl that T_C is proportional to the hole concentration. Experimentally, it was reported that Mn doped $CuGaTe_2$ is FM semiconductor with T_C of 240 K [26].

The band structure of $CuMn_xGa_{1-x}S_2$ for $x = 0.125$, plotted in Fig. 4, shows that the system is half-metallic with about a 1 eV band gap existing in the spin-down channel. This is particularly useful in view of spin-injection applications: holes in proximity of E_F, i.e. the relevant energy range for injection, will have a well-defined spin. The band structure also confirms that Mn doping also

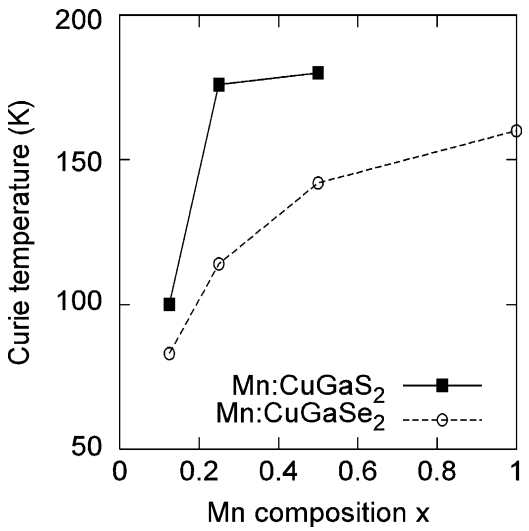

Fig. 3. The estimated Curie temperature for Mn doped $CuGaSe_2$ and $CuGaS_2$ as a function of the Mn concentration.

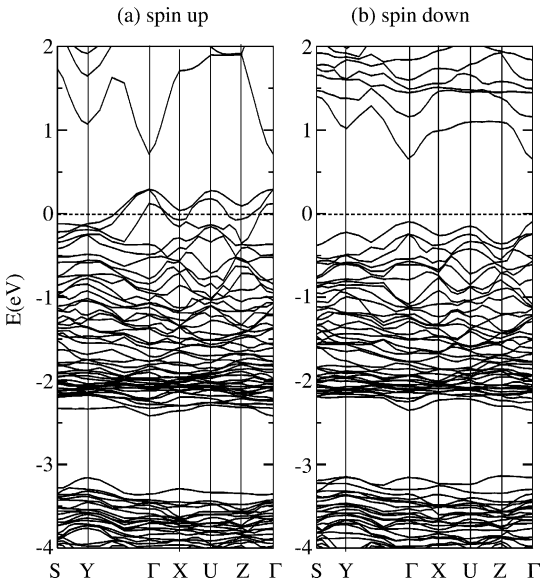

Fig. 4. (a) Spin up and (b) spin down band structures of $CuMn_xGa_{1-x}S_2$ for $x = 0.125$.

provides hole-like carriers in these systems, and thus stabilizes the FM coupling between Mn ions.

4. Magnetic interaction in Mn_xGe_{1-x}

Recently, a number of investigators have noticed that the disorder of Mn site locations might play an important role: [9,27–29] disorder was found to enhance the FM transition temperature in both the mean-field approximation and from an analysis of the zero-temperature spin stiffness [27]. Experimentally, it is also well-known that the electronic and magnetic properties are strongly affected by the temperature or duration of annealing [29–31]. For example, large variations of T_C, from 49 to 111 K in $Ga_{1-x}Mn_xAs$ at $x = 6–8\%$ were found when it is annealed at different temperatures in a narrow temperature range, from 282 to 350 K [29]. For Mn_xGe_{1-x}, T_C was found to be as high as 274 K in a very recent work [32], in contrast with up to 116 K found previously. Recent experimental work [4] demonstrated the control of FM order of Mn_xGe_{1-x} through application of a ~0.5-V gate voltage, showing the potential application of Mn_xGe_{1-x} in microelectronic technology.

To gain insights into the magnetic interaction responsible for ferromagnetism observed in Mn_xGe_{1-x}, we have carried out highly-precise all-electron FLAPW [16] calculations on large supercells as a function of Mn–Mn distances for different Mn site locations [33]. Here, we report that the coupling between Mn atoms is not always FM even for large Mn distances. The magnetic order in Mn_xGe_{1-x} strongly depends on the Mn site locations due to a RKKY-like interaction between the localized Mn ions. Our results serve to explain the experimental effective magnetic moments and the observed large range of Curie temperature in Mn_xGe_{1-x}. They also indicate that a higher Mn concentration enhances the exchange interactions and thus the Curie temperature.

We employed an a^3 supercell (a is the cubic lattice constant), with 62 Ge atoms and 2 Mn atoms, to simulate the effect of local disorder of the Mn distributions, with Mn–Mn distances ranging from 2.45 to 9.80 Å. All six cases are described in Table 4, with a system notation for each case, consisting of three digits following N to represent (x, y, z) coordinates in units of $a/4$ of the second Mn (the first is at the origin). The total energy results indicate that the Mn pair does not prefer either the nearest neighbor (N111 case), nor the uniform distribution with the largest Mn–Mn separation distance (N444 case). Instead, the FM N440 case with the Mn–Mn separation of 8.0 Å has the lowest energy. Surprisingly, the Mn_xGe_{1-x} is not always FM even at large Mn–Mn distances (see Table 4). For the nearest neighbor situation (case N111), AFM is strongly preferred, as found in other calculations [4]. However, the AFM states for N400 and N444 are clearly lower than the FM state by energy of 22.4, 37.5 meV, respectively, which are larger than the error (~10 meV/Mn) of our calculations. Therefore, the mechanism for the ferromagnetism in Mn_xGe_{1-x} is not simply from the competition between a long-range FM interaction and a short-range AFM interaction, as supposed in Ref. [4].

Now, according to RKKY theory [34], the interaction between two localized moments through the induced spin density has the form of

$$H = -\frac{J^2}{g^2\mu_B^2 V}\sum_q \chi(\mathbf{q})e^{iq\cdot r}\mathbf{S}_\alpha\mathbf{S}_\beta, \quad (3)$$

Here J is the exchange integral between conduction electrons and the electron localized at the impurity, and $\chi(\mathbf{q})$ is the magnetic susceptibility of the conduction electrons. It is well-known that if $\chi(\mathbf{q})$ is treated as for free electrons that the RKKY Hamiltonian could be rewritten as

$$H \propto \sum_q \chi(\mathbf{q})e^{iq\cdot r}\mathbf{S}_\alpha\mathbf{S}_\beta \propto [\sin(2k_F r) - 2k_F r\cos(2k_F r)]/r^4, \quad (4)$$

where k_F is the Fermi wave vector corresponding to the average density $\bar{\rho}$. Consider now the RKKY Hamiltonian for two situations, $\mathbf{S}\alpha$, $\mathbf{S}_\beta$ with parallel and opposite directions, which will have the same expression as in Eq. (4) except for their signs. Therefore, the energy difference between the AFM and FM state of the two localized moments system,

Table 4
The FLAPW calculated total energy (relative to the lowest energy N440 FM case), the AFM and FM energy difference, for the different Mn locations from the $Ge_{62}Mn_2$ supercell. One Mn is put at (0,0,0), while the other Mn position is listed at the table. The expression of exchange constants for the AFM and FM energy difference is also listed in the last column. The details for the expression are explained in the text

System	Mn_2 Position (a)	Mn–Mn dist (Å)	E_{FM} (meV/Mn)	E_{AFM} (meV/Mn)	$E_{AFM} - E_{FM}$ (meV/Mn)	$= \Sigma J(r)$
N111	(1/4,1/4,1/4)	2.45	290.3	2.7	−287.6	J_{111}
N220	(1/2,1/2,0)	4.00	12.2	93.6	81.4	J_{220}
N400	(1,0,0)	5.66	67.9	45.5	−22.4	$2J_{400}$
N224	(1/2,1/2,1)	6.93	75.9	68.8	−7.1	$2J_{224}$
N440	(1,1,0)	8.00	0	103.1	103.1	$4J_{440}$
N444	(1,1,1)	9.80	106.8	69.3	−37.5	$8J_{444}$

which is exactly the $J(r)$ discussed above, is also proportional to the right side of Eq. (4).

We now fit the calculated exchange interaction $J(r)$ with Eq. (4), taking k_F as a parameter. The fitted curve shown in Fig. 5. as the solid line, shows excellent agreement between the calculated $J(r)'$s and the RKKY model. It is not appropriate to estimate k_F from the hole concentrations because the holes are mostly contributed by Mn 3d and nearby Ge 4p electrons, and thus are localized at Mn sites.

The magnetic moments are localized at Mn sites, while only around 0.06 μ_B within muffin-tin spheres of the Ge nearest to Mn, (0.05 μ_B for the AFM case) opposite to the direction of Mn moment. The moments at Ge sites decreases rapidly to zero as the distance increases. That the Ge 4s and 4p electrons prefer AFM alignment to the nearby Mn 3d is similar to the As 4s and 4p in (Ga,Mn)As [23]. The total density of states (DOS) of FM N440 (not shown), indicates that the system is half-metallic—consistent with the average integer magnetic moments of 3 μ_B/Mn.

As done for the $CuGa_{1-x}Mn_xSe_2$ system [21], we employ Monte Carlo simulation results for estimation of T_C by $T_C = 0.447|J_1|$ [25], where J_1 is the exchange constant for the nearest neighbor interaction of the local magnetic ions. The estimated T_C is $\sim$134 K for the energetically preferred N440 case (with $J_1 = 25.8$ meV), and it could be up to $\sim$400 K for Mn atoms located as in the N220 case (with $J_1 = 81.4$ meV), and so appear to be is in good agreement with the experimental results, 116 K [4] and 274 K [32] obtained by different groups. The larger T_C for the N220 case confirms results from the mean-field approximation and an analysis of the zero-temperature spin stiffness that Mn disorder may enhance the FM transition temperature [27,28].

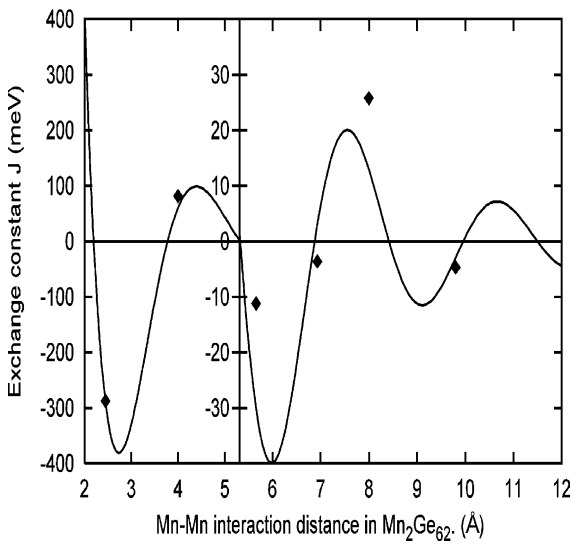

Fig. 5. The exchange interaction, J_n, for the Mn atoms versus their distance in Mn_xGe_{1-x}, where the J_n's are defined with the convention $|\mathbf{S}| = 1$. The solid line is the RKKY model fitted with $k_F = 1.02$ Å^{-1}.

In addition, the effective magnetic moment in Mn_xGe_{1-x} may be estimated from the calculated total energies which mostly lie within 100 meV/Mn higher than the N440 FM case, as listed in Table 4. The calculated magnetic moment is 3.0 μ_B per Mn for all systems except for the FM N111 case (3.12 μ_B per Mn). Now, the saturation magnetization obtained from the experimental magnetization loops are up to 30 emu/cm^3 for $Mn_{0.02}Ge_{0.98}$, corresponding to 1.4–1.9 μ_B/Mn if all Mn atoms contribute equally [4]. This means that only $\sim$50% Mn are magnetically active if each Mn atom has the theoretical moment of 3 μ_B. Since the Mn locations are rather random due to their competitive total energies and the magnetic moments of Mn are not 'active' in some cases, like N111 and N400, due to the AFM state being preferred, this may explain why the experimental magnetic moments are much smaller than the theoretical values. As a crude estimate, we assume that the Mn are distributed in the six cases listed in Table 4 with relative weights given by a Boltzmann factor, $e^{-\Delta E_i/KT}$. Considering that the annealing temperature for Mn_xGe_{1-x} sample synthesis in Park's work is around 340 K [4], it corresponds an effective magnetic moment of 1.7 μ_B/Mn and is in excellent agreement with experiment (1.4–1.9 μ_B/Mn).

Acknowledgements

Work supported by DARPA/ONR (grant No.: N00014-02-1-0887) and grants of computer time at the NAVO and ERDC Supercomputing Centers. The authors thank Dr Picozzi, Dr Shishidou for their helps and discussions.

References

[1] S.A. Wolf, et al., Science 294 (2001) 1488.
[2] H. Ohno, Science 281 (1998) 951.
[3] G.T. Thaler, et al., Appl. Phys. Lett. 80 (2002) 3964.
[4] Y.D. Park, et al., Science 295 (2002) 651.
[5] G.A. Medvedkin, et al., Jpn. J. Appl. Phys. 39 (2000) L949.
[6] Y.-J. Zhao, S. Picozzi, A. Continenza, W.T. Geng, A.J. Freeman, Phys. Rev. B 65 (2002) 094415.
[7] S. Cho, et al., Phys. Rev. Lett. 88 (2002) 257203.
[8] T. Sasaki, et al., J. Appl. Phys. 91 (2002) 7911.
[9] P. Korzhavyi, et al., Phys. Rev. Lett. 88 (2002) 187202.
[10] T. Dietl, H. Ohno, J. Cibert, D. Ferrand, Science 287 (2000) 1019.
[11] J. Inoue, S. Nonoyama, H. Itoh, Phys. Rev. Lett. 85 (2000) 4610.
[12] J. Furdyna, J. Kossut (Eds.), Diluted Magnetic Semiconductors, Semiconductors and Semimetals, vol. 25, Academic Press, Boston, 1986.
[13] Y.-J. Zhao, W.T. Geng, A.J. Freeman, T. Oguchi, Phys. Rev. B 63 (2001) 201202.

[14] P. Mahadevan, A. Zunger, Phys. Rev. Lett. 88 (2002) 047205.
[15] D. Ferrand, et al., Phys. Rev. B. 63 (2002) 085201.
[16] E. Wimmer, H. Krakauer, M. Weinert, A.J. Freeman, Phys. Rev. B 24 (1981) 864.
[17] J.P. Perdew, K. Burke, M. Ernzerhof, Phys. Rev. Lett. 77 (1996) 3865.
[18] B. Delley, J. Chem. Phys. 113 (2000) 7756.
[19] S.B. Zhang, J.E. Northrup, Phys. Rev. Lett. 67 (1991) 2339.
[20] S.B. Zhang, S.-H. Wei, A. Zunger, H. Katayama-Yoshida, Phys. Rev. B. 57 (1998) 9642.
[21] Y.-J. Zhao, A.J. Freeman, J. Magn. Magn. Mater. 246 (2002) 145.
[22] S. Picozzi, J. Zhao, A.J. Freeman, B. Delley, Phys. Rev. B 66 (2002) 205206.
[23] Y.-J. Zhao, W.T. Geng, K.T. Park, A.J. Freeman, Phys. Rev. B 64 (2001) 035207.
[24] A. Twardowski, H.J.M. Swagten, W.J.M. de Jonge, Phys. Rev. B 36 (1987) 7013.
[25] H.T. Diep, H. Kawamura, Phys. Rev. B 36 (1987) 7013.
[26] W.-L. Lee, T. Pray, K.A. Regan, R.J. Cava, R.N. Bhatt, N.P. ONG, APS March meeting U16.4, Indianapolis, USA, 2002
[27] M. Berciu, R.N. Bhatt, Phys. Rev. Lett. 87 (2001) 107203.
[28] A.L. Chudnovskiy, D. Pfannkuche, Phys. Rev. B 40 (2002) 7019.
[29] K.M. Yu, et al., Phys. Rev. B 66 (2002) 201303.
[30] T. Hayashi, Y. Hashimoto, S. Katsumoto, Y. Iye, Appl. Phys. Lett. 78 (2001) 1691.
[31] S.J. Potashnik, et al., Appl. Phys. Lett. 79 (2001) 1495.
[32] S. Cho, et al., Phys. Rev. B 66 (2002) 033303.
[33] Y.-J. Zhao, T. Shishidou, A.J. Freeman, Phys. Rev. Lett. 90 (2003) 047204.
[34] R.M. White, Quantum Theory of Magnetism, McGraw-Hill, 1970.